INTERNATIONAL JOURNAL OF METACENTRE
MARITIME APPLICATION, TECHNOLOGY, ENGINEERING, AND TRANSPORTATION
http://ijm-nasp.unhas.ac.id. eISSN : 2809-8307

Study of the Impact of Biofouling on Ship Resistance Using Autodesk CFD

Rosmani[1], Suandar Baso[2*], Heri Saputra[3], Muhammad Akbar Asis[4], Lukman Bochary[5], Sopyan Chalil[6]

[1,2,4,5]*Department of Naval Architecture, Faculty of Engineering, Hasanuddin University, Indonesia*
[3]*Student of Naval Architecture, Facultyof Engineering, Hasanuddin University, Indonesia*
[6]*PT. Industri Kapal Indonesia (IKI Makassar)*

Received: 20/02/2023
Revised: 25/03/2023
Accepted: 15/05/2023
Published:28/06/2023

* Corresponding author:
s.baso@eng.unhas.ac.id

Abstract

Biofouling, the accumulation of marine organisms on ship hulls, poses a substantial challenge in the maritime industry. Over time, organisms like algae and molluscs adhere to hull surfaces, creating a biofouling layer that disrupts water flow and increases ship resistance. This study investigates the effects of biofouling on ship resistance and fluid flow patterns along the hull. Data collection involved measuring key ship dimensions, analyzing ship lines plan drawings, and measuring biofouling thickness. Autodesk Computational Fluid Dynamics (CFD) software was used to calculate ship resistance and analyze fluid flow along the hull. Two conditions were compared: a hull without biofouling and a biofouled hull. At a speed of 1.220 m/s, the biofouled ship model exhibited a resistance of 3,739 N, while the clean hull had a resistance of 3,280 N, indicating a 13.642% resistance increase due to biofouling. Fluid flow analysis revealed complex flow patterns along the biofouled hull, potentially reducing operational efficiency. These findings underscore the importance of biofouling prevention and control measures in minimizing resistance and maintaining operational efficiency. A deeper understanding of fluid flow characteristics related to biofouling allows ship operators and companies to make informed decisions about ships maintenance, reducing environmental impacts and operational costs. This research contributes to addressing biofouling challenges in the maritime industry.

Keywords: Biofouling; Ship Resistance; Fluid Flow; Maritime Industry; Prevention

1. Introduction

In general, when an object remains submerged in seawater for an extended period, it is prone to developing a condition where various marine organisms adhere to its surface. This phenomenon, commonly observed on ship hulls, is known as biofouling. Biofouling occurs as a result of biological contamination by marine organisms during a ship's voyage.

The accumulation of marine organisms, or biofouling, on a ship's hull surface can have detrimental effects on both its economic and operational aspects. Biofouling alters the surface roughness of the hull, thereby significantly increasing the ship's resistance as it moves through the water. Resistance, in this context, includes various components, with frictional resistance being a significant contributor. When biofouling attaches to the ship's underwater hull and propeller, it effectively roughens these surfaces, leading to higher resistance and increased fuel consumption. Consequently, the cost of fuel rises. Additionally, biofouling can affect the ship's volume (displacement), reduce its speed, and disrupt the flow pattern during sailing.

According to Curtin [1], a biofouling layer measuring 200 μm on a ship's hull can reduce its speed by up to 20%, resulting in substantial losses. Another theory, proposed by Maley, suggests that after 6-8 months of sailing with biofouling, a ship's speed can decrease by up to 50%, leading to a 40% increase in fuel consumption. This reduced speed also results in a delay of 10-15% in the total sailing time [2]. Experimental research conducted by Yusim [3] indicates that biofouling growth over a year increases the total resistance by 36.65% for ships with uniform biofouling growth on their entire wetted surfaces and by 47.11% for ships with irregular biofouling growth.

Computational Fluid Dynamics (CFD) has gained popularity for predicting ship resistance due to its efficiency and cost-effectiveness. Software such as Autodesk CFD is employed to simulate pressure distribution and fluid velocity around a ship, using the Navier-Stokes equations solved with the Finite Element Method (FEM) [4].

In this context, CFD, particularly Autodesk CFD software, has become an invaluable tool for assessing the impact of biofouling on ship resistance. CFD allows for the simulation of pressure distribution and fluid velocity around the ships, facilitating a detailed analysis of changes in resistance caused by biofouling.

Yigit's study [5] introduces a novel CFD-based unsteady RANS model, successfully elucidating the effects of various biofouling conditions and marine coatings on ship performance. The findings reveal that even thin layers of biofouling or damaged coatings can significantly increase fuel consumption and the power required to propel the ships. Moreover, the influence of hull roughness on ship resistance and wave dynamics plays a pivotal role, enhancing our understanding of fluid dynamics around biofouled ships. These findings offer valuable insights for the maritime industry, aiding in biofouling management and the design of more efficient ships.

Soonseok Song's research [6] further emphasizes the complexity of biofouling's impact on ship resistance, demonstrating variations based on ships type, size, and speed. The study identifies two key factors influencing this impact: the thickness of the biofouling layer (relative roughness height) and the flow characteristics around the ship's surface (roughness Reynolds number). These findings underscore the importance of effective biofouling management in designing efficient ships, with the potential to make substantial contributions to the maritime industry by improving performance and reducing environmental impact.

Lastly, [7] investigates the increase in skin friction resistance resulting from biofouling-induced alterations in surface roughness. Using two-dimensional flat plate models and CFD analysis, this research explores variations in roughness length scale. The results indicate an increase in skin friction resistance ranging from 3.5% to 206.9%, depending on the model type and surface roughness. These findings provide valuable insights into the impact of biofouling on ships operational efficiency and the environment.

This paper aims to conduct an in-depth study using Autodesk CFD software to assess the impact of biofouling on ship resistance. The research aims to enhance our understanding of how biofouling affects ships performance, particularly in terms of resistance, thereby offering improved guidance for biofouling management and the design of more efficient ships.

2. Methods

Autodesk CFD software performs Computational Fluid Dynamics (CFD) simulations, enabling engineers and analysts to make informed predictions regarding the behavior of liquids and gases [8]. This CFD software employs the finite element method (FEM), which is a numerical technique for solving partial differential equations (PDEs) in two or three spatial dimensions. It results in a system of algebraic equations for the dependent variable at discrete points or nodes on each element. Similarly, it analyzes a physical object by dividing it into numerous finite elements using the finite element analysis (FEA), a computerized analytical method. Autodesk CFD primarily uses FEM due to its ability to model various geometric shapes, including linear and 3D tetrahedral elements (unstructured grids). This maintains the inherent geometric flexibility within Autodesk CFD [4]

The core equations that dictate the behavior of fluid flow pertain to the incompressible external Navier-Stokes or momentum equations [9]. The PDEs that represent the continuity equation can be expressed in the following manner:

$$\frac{\partial \rho}{\partial t} + \frac{\partial \rho u}{\partial x} + \frac{\partial \rho v}{\partial y} + \frac{\partial \rho w}{\partial z} = 0 \tag{1}$$

Where, ρ is the density, t is the time, u is the velocity component in x-direction, v is the velocity component in y- direction, and w is the velocity component in z-direction.

Subsequently, equations for X-Momentum, Y-Momentum, and Z-Momentum are derived based on the continuity equation in the following manner.

The X-Momentum equation is provided as follows:

$$\begin{aligned}&\rho \frac{\partial u}{\partial t} + \rho u \frac{\partial u}{\partial x} + \rho v \frac{\partial u}{\partial y} + \rho w \frac{\partial u}{\partial z} \\ &= \rho g_x - \frac{\partial u}{\partial t} + \frac{\partial u}{\partial x}\left[2\mu \frac{\partial u}{\partial x}\right] + \frac{\partial u}{\partial y}\left[\mu\left(\frac{\partial u}{\partial y} + \frac{\partial u}{\partial x}\right)\right] + \frac{\partial u}{\partial z}\left[\mu\left(\frac{\partial u}{\partial z} + \frac{\partial w}{\partial x}\right)\right] \\ &+ S_\omega + S_{DR}\end{aligned} \tag{2}$$

The Y-Momentum equation is provided as follows:

$$\begin{aligned}&\rho \frac{\partial v}{\partial t} + \rho u \frac{\partial v}{\partial x} + \rho v \frac{\partial v}{\partial y} + \rho w \frac{\partial v}{\partial z} \\ &= \rho g_y - \frac{\partial p}{\partial y} + \frac{\partial}{\partial x}\left[\mu \frac{\partial u}{\partial y} + \frac{\partial v}{\partial x}\right] + \frac{\partial}{\partial y}\left[2\mu \frac{\partial v}{\partial x}\right] + \frac{\partial}{\partial z}\left[\mu\left(\frac{\partial v}{\partial z} + \frac{\partial w}{\partial y}\right)\right] \\ &+ S_\omega + S_{DR}\end{aligned} \tag{3}$$

The Z-Momentum equation is provided as follows:

$$\begin{aligned}&\frac{\partial w}{\partial t} + \rho u \frac{\partial w}{\partial x} + \rho v \frac{\partial w}{\partial y} + \rho w \frac{\partial w}{\partial z} \\ &= \rho g_z - \frac{\partial p}{\partial z} + \frac{\partial}{\partial x}\left[\mu \frac{\partial u}{\partial z} + \frac{\partial w}{\partial x}\right] + \frac{\partial}{\partial y}\left[\mu\left(\frac{\partial v}{\partial z} + \frac{\partial w}{\partial y}\right)\right] + \frac{\partial}{\partial z}\left[2\mu \frac{\partial w}{\partial z}\right] \\ &+ S_\omega + S_{DR}\end{aligned} \tag{4}$$

Where, g_x, g_y, g_z are the gravitational acceleration in x, y, z direction, μ is the viscosity, S_ω rotating flow, and S_{DR} is the distributed resistance term.

The momentum equation contains two source terms, S_ω for the rotating coordinate and S_{DR} for distributed resistance. The general expression for the distributed resistance term is as follows:

$$S_{DR} = -\left(K_i + \frac{f}{D_H}\right)\frac{\rho V_i^2}{2} - C\mu V_i \quad (5)$$

Where, V represents the velocity, i denotes the global coordinate direction (u, v, w momentum equation), f stands for the friction factor, d signifies the hydraulic diameter, and C denotes the permeability. The K-factor term can be applied to a single momentum equation at a time since each direction possesses its distinct K-factor. The other two types of resistance affect each momentum equation equally

$$S_\omega = -2\rho\omega_i \text{ x } V_i - \rho\omega_i \text{ x } \omega_i \text{ x } r_i \quad (6)$$

Where, ω is the rotational speed and r is the distance from axis of rotation.

For turbulence models, this study uses the wall function or $k - epsilon$ $(k - \varepsilon)$, k is the kinematic energy per unit mass and ε is the turbulent dissipation wherein it is suitable for the interaction of the externa; incompressible flow with complex geometry.

The research investigating the influence of biofouling on ship resistance focuses on a specific passenger ship known as KM. Wilis, which is operated by PT. Pelayaran Nasional Indonesia (National Indonesian Shipping). This ship is currently undergoing its annual maintenance at PT. Industri Kapal Indonesia (Indonesian Ship Industries). To conduct this study, it's crucial to have a clear understanding of the ship's main dimensions, which are summarized in Table 1.

Tabel 1. Main dimension ship.

No.	Items	Value	Unit
1	Length Over All (LOA)	74,00	m
2	Length Between Perpendicular (LBP)	68,00	m
3	Breadth (B)	15,20	m
4	Depth (D)	6,00	m
5	Draft (d)	2,85	m
6	Speed (V)	9	knot
7	Displacement (Δ)	2,090	ton

In this research, the distribution of biofouling on the sample ship will be modeled using Maxsurf Pro Modeler and Rhinoceros software. Therefore, direct measurements of biofouling thickness are required using equipment such as a tape measure, ruler, and spike. Biofouling thickness measurements will be conducted after the ship has been sailing for one year, and measurements will be taken at 182 points distributed on both sides of the ship. The locations of measurement points can be seen in Figure 2.

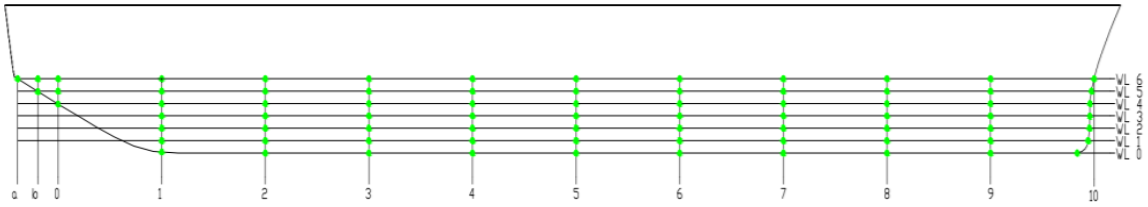

Figure 2. Biofouling thickness measurement points.

The hull shape modeling is performed using Maxsurf Pro Modeler software based on the lines plan while considering geometric and dynamic aspects. After the hull shape is modeled, the next step is to model the biofouling thickness based on measurement results. Rhinoceros software is used to generate the biofouling thickness model by duplicating the lower side of the ship's hull below the waterline. Subsequently, to transform the smooth surface into a rough surface, a surface modification process is carried out (rebuild surface). The results of the modeling, depicting the conditions with and without biofouling or smooth and rough hulls, can be seen in Figure 3.

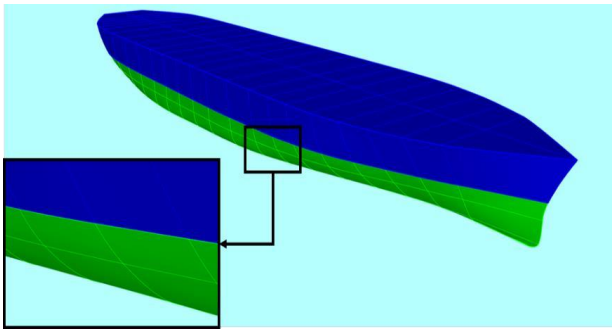

(a)

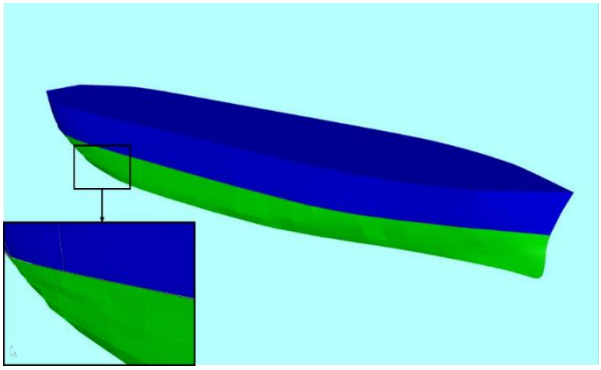

(b)

Figure 3. (a) Model without biofouling and (b) with biofouling.

After the ship is modeled with biofouling on the hull, the next step is the analysis phase using Autodesk CFD. The initial step involves modeling an experimental tank with dimensions of 5L in length, 2.2L in width, and 1.5L in height, as shown in Figure 4. Subsequently, boundary conditions will be determined by inputting velocity data ranging from 5 to 15 knots at the inlet, pressure at the outlet, and symmetry conditions on the experimental tank walls.

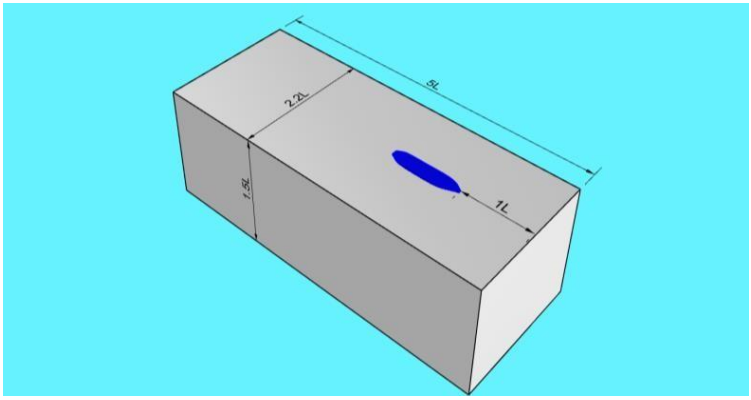

Figure 4. Visualization of the model and boundary layer dimensions.

After setting the boundary conditions, the next step is the Meshing phase for each of the two hull surface conditions. The final stage in the analysis is the Solve phase, taking into account the convergence results of residual in and residual out with a residual out success threshold of 10^{-8}.

Before initiating the Solve process, a control step is performed to ensure desired outcomes and to determine the physical characteristics of the fluid flow. This includes selecting the solution mode, the number of iterations, result quantities, determining automatic convergence assessment, compressibility flow, and turbulence. In this research, the solution mode employed is steady-state fluid flow with a total of over a thousand iterations per ship speed, and the type of fluid flow used is turbulent with the standard k-epsilon (k-ϵ) model equation.

Upon completion of the Solve process, the obtained results can be viewed in the "results" menu. The desired outcomes in this study encompass the visualization of fluid flow velocity (velocity magnitude), static pressure, ship resistance values (drag force), ship resistance coefficients, as well as the fluid flow characteristics along the ship's hull.

3. Result and Discussion

3.1. Visualization of velocity magnitude

The Visualization of velocity magnitude provides insights into the speed of fluid flow along the hull of the ship model. This visualization plays a pivotal role in evaluating its influence on the resistance generated by fluid motion. The velocity magnitude visualization along the ship's hull is extracted from the results obtained in the plane menu, employing a colour scale ranging from 0 m/s to 1.3 m/s. Figure 5 depicts the velocity magnitude visualization at a velocity of 1.220 m/s.

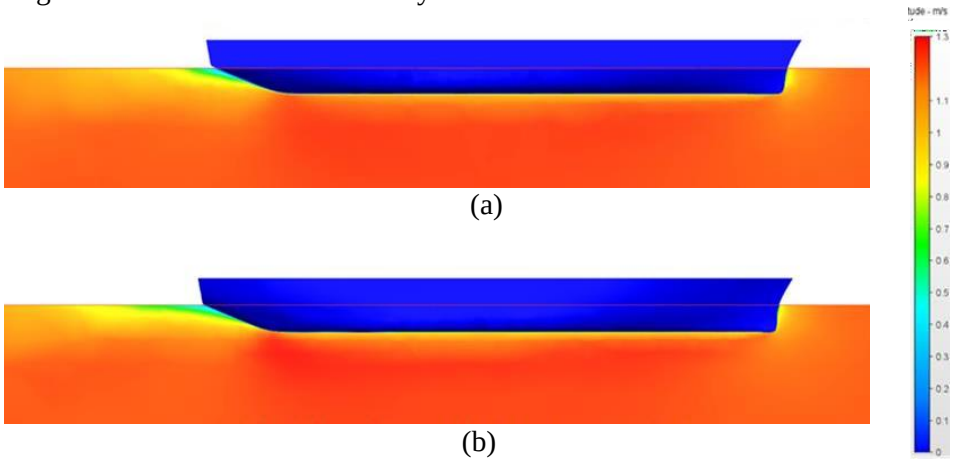

(a)

(b)

Figure 5. Visualization of ship model velocity magnitude at as speed of 1.220 m/s (a) Model without biofouling and (b) with biofouling.

It is evident that the velocity magnitude along the hull of the ship model coated with biofouling exhibits relatively low values, as indicated by the colour gradient transitioning from yellow to green and blue along the bottom and stern sections, with velocities ranging between 0.3-0.9 m/s. This observation highlights that the velocity magnitude of fluid flow around the biofouling-coated model hull is comparatively lower than that of the model without biofouling. The variation in colour gradients underscores the differences in values influenced by the hull contour and the flow velocity over the hull surface. Consequently, this results in increased viscosity forces and momentum losses, leading to relatively higher values of viscosity resistance and drag coefficient.

In the lateral section of the ship model's hull coated with biofouling, a noticeable reduction in velocity is observed due to the presence of biofouling thickness or contours that impede the fluid flow. This phenomenon is clearly depicted in the velocity vectors shown in Figure 6.

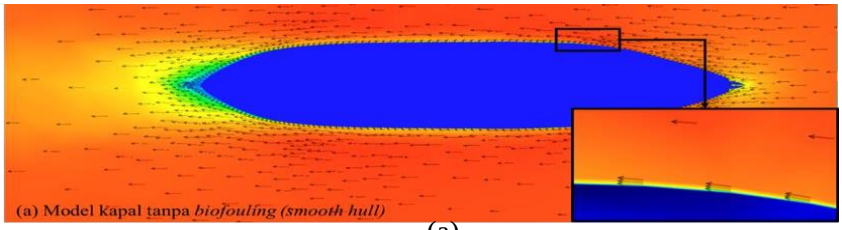

(a)

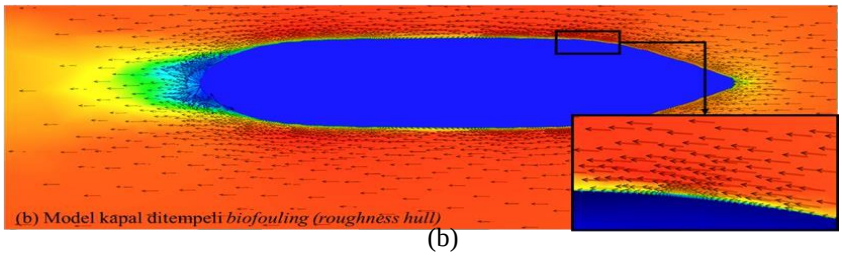

(b)

Figure 5. Visualization of ship model velocity magnitude at as speed of 1.220 m/s, (a) Model without biofouling and (b) with biofouling.

Based on Figure 6, it can be inferred that in the lateral section of ship model's hull without biofouling, the fluid flow exhibits laminar behaviour, closely following the streamline patterns of the ships hull. Conversely, on the lateral and stern sections of the ship model coated with biofouling, turbulent flow occurs due to the rough surface caused by biofouling. Consequently, the fluid flow deviates from the streamline patterns of the ship's hull, leading to disturbance evident in the colour gradient shift from yellow to green. The predicted velocity values fall within the range of 0.7 to 0.9 m/s.

3.2. Visualization of static pressure

In the bow and stern sections of the ship, fluid flow at a specific velocity leads to changes in the distribution of static pressure in those areas. This enables us to identify the parts of the model experiencing turbulence and those experiencing the most significant resistance due to the model's speed and hull shape below the waterline. The visualization of simulations results regarding static pressure can be found in Figure 7 and 8.

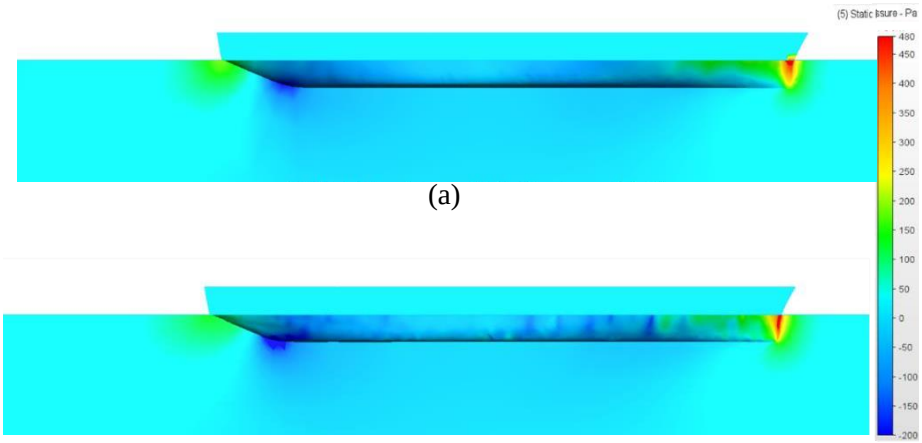

(a)

(b)

Figure 7. Visualization of ship model static pressure at as speed of 1.220 m/s at longitudinal view (a) Model without biofouling and (b) with biofouling.

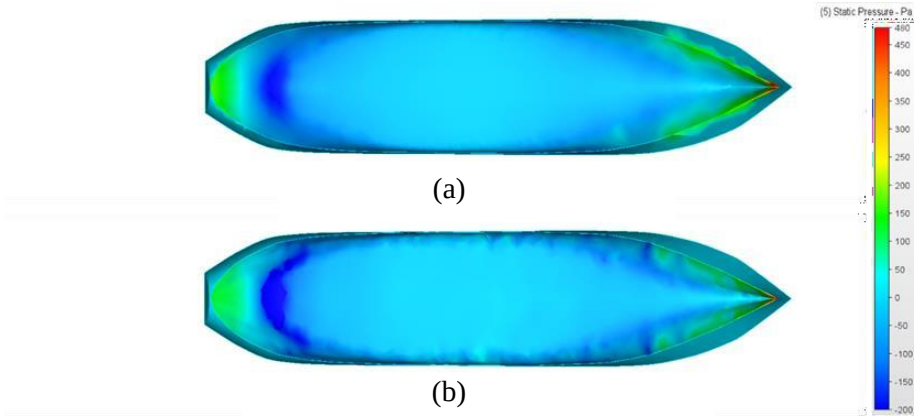

(a)

(b)

Figure 8. Visualization of ship model static pressure at as speed of 1.220 m/s at bellow view (a) Model without biofouling and (b) with biofouling.

It is observed that the distribution of static pressure on the bow section the ship model coated with biofouling (roughness hull) tends to be relatively low, as indicated by the subtle colour gradient changes from read, orange, yellow, to green in the bow area, compared to the model without biofouling. With a large surface area, which significantly affects the distribution of static pressure. This phenomenon is attributed to reduced fluid velocity on the ship model coated with biofouling due to the rough contour of the hull surface, resulting in relatively lower pressures experienced by the ship model's hull. This aligns with the theory that an increase in ship speed will also increase static pressure distribution, or vice versa.

Meanwhile, for the distribution of static pressure on the parallel middle body to the stern section of the ship model coated with biofouling, it is also relatively low compared to the model without biofouling, as evident from the gradual colour changes from light blue to dark blue along the model's hull, with a predicted pressure value range of -200 to -40 Pa. Consequently, there exists a significant difference in static pressure

distribution between these two models, which impacts the magnitude of pressure drag and coefficient of drag force along the ship model's hull.

3.3. Comparison of ship model resistance

In the context of ship design, it is crucial to evaluate the hydrodynamic performance of different hull configurations to optimize efficiency and reduce resistance. This study focuses on comparing the resistance characteristics of with biofouling and without biofouling across various velocity settings, as detailed in Table 4. The relationship between velocity and resistance for both hull models is graphically illustrated in Figure 9.

Tabel 4. Comparison of resistance values between with biofouling and without biofouling ship models

No.	Froud Number	Speeds (m/s)	Resistance (N)		Persentase (%)
			with biofouling	without biofouling	
1	0.097	0.407	0.434	0.543	20.117
2	0.136	0.569	0.803	0.935	14.108
3	0.175	0.732	1.276	1.440	11.431
4	0.214	0.895	1.842	2.088	11.794
5	0.253	1.057	2.506	2.852	12.121
6	0.292	1.220	3.280	3.739	12.280
			Average		**13,642**

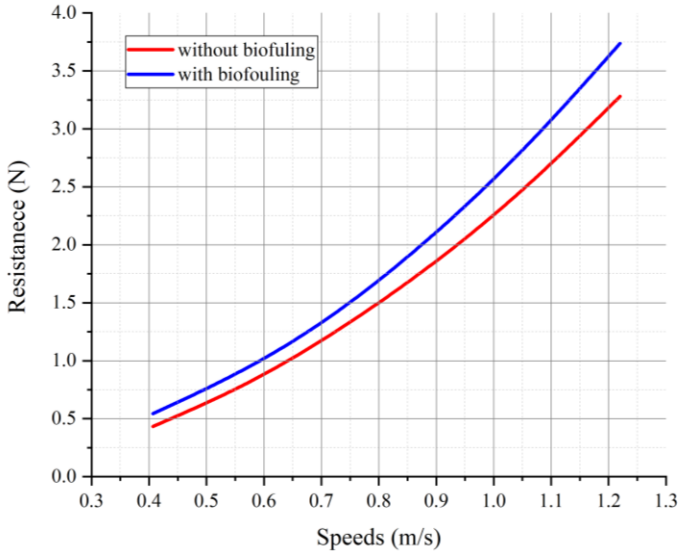

Figure 9. Compared resistance model ship's with biofouling and without biofouling.

Based on the data in Tabel 4 and Figure, the analysis of resistance resulting from biofouling growth over a one-year period reveals significant difference in resistance values between the ship models affected by biofouling and without biofouling, with an average resistance increase of approximately 13.64%. This difference in resistance values can be explained by the utilization of roughness models on the surface of the befouled ship, leading to increased frictional resistance.

However, these analysis results show a significant contrast with the results of CFD simulations, which divided the biofouling modelling into three zones: the bow, midship and stern, with percentage increase in resistance of 27.5%. Additionally, experimental research conducted by Yusim (2016) also note an approximate 30% increase in total resistance due to biofouling growth over a one-year period. This underscores that factors such as ship operational conditions and voyage routes play a crucial role in the level of biofouling growth, ultimately affecting ship resistance increases.

4. Conclusions

In conclusion, the results of numerical analysis of ship resistance and fluid flow characteristics using Autodesk CFD software indicate that the attachment of biofouling to the ship's hull (roughness hull) leads to a significant increase in ship resistance values across various speed variations. The average percentage increase in resistance for the biofouled ship model is approximately 13.64%, as compared to the model without biofouling (smooth hull). Furthermore, alterations in fluid flow characteristics are observed in the biofouled ship model, characterized by turbulence and denser flow patterns compared to the model without biofouling. These findings underscore the significant impact of biofouling on ship resistance and fluid flow, which are relevant for ship operational planning and management.

Acknowledgements

The authors would like to express their gratitude to the Engineering Faculty of Hasanuddin University for providing research grant support through the Lab-Based Education (LBE) Research scheme in 2023, which made this research possible. Additionally, the authors wish to extend their thanks to Heri Saputra and other members of the Hydrodynamic Laboratory, as well as to PT. Industri Kapal Indonesia (IKI Shipyard), for their generous assistance in data collection and analysis.

References

[1] M. E. Curtin, "Trying to Solve the Biofouling Problem," Nature Biotechnology. Access : https://www.nature.com/articles/nbt0185-38.pdf

[2] M. N. Nurrohman, "Boundary Layer Analysis to Determine Marine Fouling Growth on Ship Hull Below the Waterline Using CFD Program," Surabaya: ITS, 2017.

[3] A. K. Yusim, "Experimental Study of the Effect of Biofouling Growth on Ship Hull on Skin Friction Drag," Surabaya: ITS, 2016.

[4] S. Baso, A. Ardianti, A. A. Rosmani, "An Extended Validation of Free CFD Application for Ship Resistance Prediction in Preliminary Design Stage," Journal of Engineering Science and Technology, vol. 16, no. 3, pp. 2544-2561, 2021.

[5] Y. K. Demirel, O. Turan, A. Incecik, "Predicting the Effect of Biofouling on Ship Resistance using CFD," Applied Ocean Research, vol. 62, Jan. 2017, pp. 100-118.

[6] S. Song, Y. K. Demirel, C. D. M. Fenech, T. Tezdogan, M. Atlar, "Fouling Effect on the Resistance of Different Ship Types," Ocean Engineering, vol. 216, Nov. 2020.

[7] S. Regitasyali, M. L. Hakim, I. K. A. P. Utama, "CFD Analysis of the Increase in Ship Resistance Due to Biofouling Growth Represented by Roughness Length Scale," IOP Conf. Series: Materials Science and Engineering, vol. 1052, 2021, p. 012034.

[8] https://www.autodesk.com/products/cfd/overview

[9] Autodesk CFD Autodesk CFD, “Learning guide: General fluid flow and heat transfer equations”. Retrieved August 21, 2019, from https://knowledge.autodesk.com/support/cfd/learn-explore/caas/CloudHelp/cloudhelp/2017/ENU/SimCFD-Learning/files/GUID-83A92AE5-0E9E-4E2D-B61F-64B3696E5F66-htm.html